Improvement in corrosion resistance of AZ91D Mg alloy in simulated body fluid by cerium-based/stearic acid composite coatings

A.P. Loperena , S.B. Saidman , I.L. Lehr

PII: S2667-2669(24)00008-2
DOI: https://doi.org/10.1016/j.corcom.2023.08.004
Reference: CORCOM 108

To appear in: *Corrosion Communications*

Received date: 8 June 2023
Revised date: 4 August 2023
Accepted date: 8 August 2023

Please cite this article as: A.P. Loperena , S.B. Saidman , I.L. Lehr , Improvement in corrosion resistance of AZ91D Mg alloy in simulated body fluid by cerium-based/stearic acid composite coatings, *Corrosion Communications* (2024), doi: https://doi.org/10.1016/j.corcom.2023.08.004

Highlights

- Cerium-based/SA composite coatings were generated onto AZ91D Mg alloy.
- The state contact angle of the cerium-based surfaces was greatly improved after the SA post-treatment.
- Cerium-based/ SA composite coatings improve corrosion resistance of Mg alloy in simulated body fluid and provide protection for several days.

Research article

Improvement in corrosion resistance of AZ91D Mg alloy in simulated body fluid by cerium-based/stearic acid composite coatings

A.P. Loperena, S.B. Saidman, I.L. Lehr*

Instituto de Ingeniería Electroquímicay Corrosión (INIEC), Departamento de Ingeniería Química, Universidad Nacional del Sur (UNS), CONICET, Bahía Blanca B8000CPB, Argentina

*Corresponding author.
E-mail addresses: ivana.l.lehr@gmail.com and ilehr@uns.edu.ar (I.L. Lehr).

ARTICLE INFO

Article history:

Received 8 June 2023

Received in revised form 4 August 2023

Accepted 8 August 2023

Available online

Abstract

Magnesium alloys have attracted attention due to their biocompatibility and biodegradability. In this work, composite coatings are developed to potentially improve the corrosion resistance of AZ91D Mg alloy in simulated physiological fluid. Cerium-based/stearic acid coatings were prepared by electrodeposition combined with a simple immersion method. The effect of stearic acid bath concentration on the contact angle and corrosion resistance of the composite coatings was evaluated. The results showed that the stearic acid treatment increased the hydrophobicity of the surfaces of the cerium-based simple coatings. The use of an appropriate stearic acid concentration is a key for the fabrication of hydrophobic surfaces. The duplex coatings were demonstrated to protect the substrate from corrosion in Ringer solution.

Keywords: Hydrophobic coating; Anticorrosive coating; Cerium; Stearic acid; Mg alloy

1. Introduction

Magnesium and its alloys are biocompatible and biodegradable materials with potential applications in the biomedical field. In the latest years, orthopaedic repairs and cardiovascular treatments have been investigated through the use of different magnesium-based devices [1,2]. Magnesium is a natural component of the human body, is non-toxic, and has the particularity of degrading completely into the human body, avoiding the need for a second surgery to remove the implant [3]. In addition, Mg alloys have good mechanical compatibility with human bone, diminishing the stress shielding effect [3,4]. However, Mg alloys need to overcome some challenges in order to be used in clinical applications. First, Mg degradation rate in physiological environments is higher than desirable [4-6]. This could lead to premature failure of the clinical device. Second, Mg corrosion process involves the formation of H_2 gas, which could retard tissue growth or cause hemolysis [5]. For these reasons, surface modification of magnesium-based materials is being studied with the purpose of delaying the degradation rate and preventing clinical issues [5,7-9].

Cerium-based films are non-toxic and have been demonstrated to protect Mg-based materials in physiological conditions [10,11]. When cerium ions are released from the coating, they combine with OH^- present in the corrosive media to form cerium oxides and hydroxides. These cerium compounds are deposited onto the substrate surface inhibiting corrosion. Therefore, cerium films are also known as self-healing [12,13]. In addition, they are useful as surface pre-treatment in duplex coatings since they improve the surface adhesion of films such as epoxy and PEO coatings [14,15].

On the other hand, hydrophobic surfaces have attracted attention for different biomedical applications due to their properties such as protein adsorption control, antibacterial activity and self-cleaning [16]. Hence, hydrophobic coatings are being studied for several clinical uses such

as control of local drug delivery, antibacterial films for implant materials, study of cellular communication (i.e. biopsy) by patterned cell growth and, recently, for personal protective equipment against COVID-19 [16,17]. In addition, hydrophobic and superhydrophobic surfaces have been investigated for corrosion control of magnesium substrates [18,19]. When a hydrophobic surface is immersed in an aqueous environment, air-pockets are formed on the surface [20]. This air would form an air film that would temporarily act as a physical barrier between the environment and the substrate [20,21]. Thus, a hydrophobic surface would be able to retard the contact of the aggressive ions with the substrate surface, enhancing the corrosion resistance of the material [21]. In this sense, the generation of a biocompatible hydrophobic coating onto magnesium alloy for a stent application would not only fulfill the need to increase the corrosion resistance of the material, but also improve the clinical performance [22,23]. The latter is due to the improvement of hemocompatibility after implantation in blood vessels by reducing the adhesion of proteins and platelets [22].

Surfaces with a water contact angle (CA) greater than 90° are known as hydrophobic, whereas surfaces with CA above 150° are known as superhydrophobic [16]. A low surface energy is a condition for a surface to be hydrophobic. One of the compounds used for the fabrication of hydrophobic surfaces is stearic acid, a fatty acid that can be mostly obtained from sunflower oil, lard and suet [24]. Stearic acid has applications in the cosmetic and pharmaceutical industries [25,26] and drug delivery [24]. Nevertheless, hydrophobic surfaces themselves have shown poor anticorrosive properties. Thus, some authors have been studying the generation of hydrophobic composite coatings. Zhang et al. reported the preparation of a TiO_2 layer loaded with silicon dioxide and post-treated with stearic acid onto AZ31 Mg alloy [27]. This superhydrophobic coating protected the alloy in NaCl solution. Liu et al. achieved the formation of a superhydrophobic and anticorrosive coating onto AZ31B Mg alloy by combining electrodeposition of a CeO_2 film followed by immersion in a stearic acid bath [18]. In addition, the formation of a cerium-based superhydrophobic film onto an aluminum alloy combining the

anti-wetting properties of the hydrophobic surface with the inhibiting properties of the cerium compounds was recently reported [28].

In our previous works, the formation of biocompatible cerium-based simple coatings onto AZ91D Mg alloy was proved to effectively protect the substrate from corrosion in physiological simulated fluid. These cerium-based coatings are characterised by a hydrophilic nature. As stated above, the hydrophobicity of the surface not only is an attractive property for biomedical applications but also enhances the anticorrosive properties of the substrate. Therefore, the aim of the present work is to improve the corrosion resistance and reduce the Mg dissolution of the cerium-based coated samples by incorporating hydrophobic properties. With this purpose, two cerium-based simple coatings previously evaluated by the authors [29,30] were modified with a stearic acid treatment. The effect of stearic acid bath concentration on the hydrophobicity and corrosion resistance of the coatings was studied. The mentioned modification may be an advance in the search for a suitable corrosion rate for Mg-based alloys for the fabrication of implants. The authors present for the first time a hydrophobic duplex coating based on stearic acid that can reduce the corrosion current by about 5 orders of magnitude in physiological simulated fluid.

2. Experimental

2.1 Materials and equipment

AZ91D Mg alloy (mass fraction: 8.978% Al, 0.6172% Zn, 0.2373% Mn, 0.2987% Si, 0.1189% Cu, 0.00256% Ni, 0.0176% Fe, 0.00164% Ca, 0.01154% Zr, balance Mg) electrodes were employed as working electrodes with an exposed area of 0.070 cm^2. Before each experiment, Mg electrodes were grounded with grinding paper #1000 and washed repeatedly with triply distilled water and acetone. Traditional three-electrode configuration was used for the electrochemical experiments. $Ag/AgCl_{sat}$ was the reference electrode and a platinum sheet was used as a counter electrode. Electrochemical measurements were carried out using

potentiostat/galvanostat AUTOLAB PGSTAT 128 N and Autolab PGSTAT 204 equipped with a frequency response analysis module (FRA module). All the employed chemicals were analytical grade.

2.2 Coatings

Firstly, two different cerium-based simple coatings previously studied were formed onto the AZ91D Mg alloy [29,30]. The RCe-HAsc inner coating was obtained from a solution containing 50 mmol/L $Ce(NO_3)_3$, 6 mmol/L H_2O_2 and 5 mmol/L $C_6H_8O_6$ (ascorbic acid) at -0.25 V during 30 min [29]. The RCeMo coating was prepared in a solution containing 30 mmol/L $Ce(NO_3)_3$, 15 mmol/L Na_2MoO_4 and 10 mmol/L $C_6H_8O_7$ (citric acid) at -0.30 V during 30 min [30]. Then, the cerium-based coated samples were immersed into stearic acid solutions (SA) of different concentrations with ethanol as solvent at 50 °C for 30 min to get the different cerium-based/SA coated samples.

2.3 Chemical and morphological characterization

The SA-modified samples were analyzed using a scanning electron microscope (dual stage ISI DS 130, SEM) equipped with energy dispersive spectrometry (EDAX 9600). The chemical composition of the coatings was studied by X-ray photoelectron spectroscopy (Specs setup operating system, XPS) and Fourier transform infrared (ATR-FTIR Nicolet iS20 spectrometer equipped with an iD7 ATR module). The XPS analysis chamber is equipped with a dual anode (Al/Mg) X-ray source and a 150-mm hemispherical electron energy analyser (PHOIBOS). The XPS spectra deconvolution was done using the CASA XPS software with a Gaussian–Lorentzian mix function. ATR-FTIR spectra were recorded in the range of 4000 – 500 cm^{-1} at a resolution of 4 cm^{-1} resolution. An optical microscope (Olympus Tokyo) was employed to observe the coating surface. The static CA with Ringer solution was measured for the unmodified and SA-modified samples. The droplet volume was 10 µL, CA was captured by digital camera and measured using ImageJ software. Three samples of each coating were

evaluated in order to obtain an average value. The peel-off test of the coatings was made using a 3M tape.

2.4 Corrosion testing

2.4.1 Electrochemical measurements

The corrosion behaviour of the coatings was evaluated in Ringer solution (composition per litre: 8.60 g NaCl, 0.30 g KCl and 0.32 g $CaCl_2 \cdot 2H_2O$) at 37 °C by the potentiodynamic method, the variation of the open circuit potential (OCP) as a function of time and the electrochemical impedance spectroscopy (EIS). Tafel tests were carried out by polarising from cathodic to anodic potentials with respect to the open circuit potential at 0.001 V s^{-1}. The impedance measurements were performed at the open circuit potential in the frequency range of 10^5 - 10^{-2} Hz with an amplitude of 10 mV. All experiments were conducted after the steady state. Each set of experiments was repeated at least three times to ensure reproducibility.

2.4.2 Hydrogen evolution

The equipment employed consisted of a beaker containing Ringer solution where the samples were immersed. The volume of the released gas was measured with the use of a funnel and a burette placed over the sample. The uncoated and coated specimens were immersed with an exposed area of 0.7 cm^2. To ensure reproducibility of the test results, the measurements were repeated at least three times.

2.4.3 Mg released

The quantity of Mg released in Ringer solution was determined by atomic absorption spectroscopy. The employed equipment was an AA Perkin Elmer Analyst 700 spectrophotometer. The covered and uncovered samples were immersed in 50 mL of Ringer solution for 5 h, then the solutions were homogenised and analysed.

3. Results and discussion

3.1 Effect of the SA bath concentration

Static CA with Ringer solution was measured to evaluate the hydrophilicity or hydrophobicity of the coated Mg surfaces. From Fig. 1(a), it can be seen that the untreated RCe-HAsc coating has a CA < 90°, indicating high hydrophilicity. Then, the SA treatment increases the CA in all cases to different extents. As the concentration of SA bath increases, the CA increases and then drops. Among the SA-treated samples, the one immersed in 0.75 mmol/L SA shows the highest value of CA (120.3°), indicating that this treated sample is the most hydrophobic. Fig. 1(b) shows the CA with Ringer solution for the RCeMo-H_3Cit simple coating untreated and treated in different SA baths. For the cerium-based coating, the CA is zero whereas the presence of SA increases the CA to values between 50° and 130°. Again, the CA increases and then drops with the increase of SA concentration. The treatment in 0.75 mmol/L SA shows a higher CA of 128.7°, proving the hydrophobicity of the surface. From the CA results, it was demonstrated that the hydrophilic cerium-based simple coating surfaces can be converted into hydrophobic surfaces by immersion treatment in SA bath. The CA measurements for both post-treated cerium-based surfaces suggest that there is an optimal SA bath concentration to generate hydrophobic surfaces. The hydrophobicity of SA coatings is related not only to the fatty nature of the compounds but also to the morphology of the surfaces [31]. After SA deposition, the ethanol evaporates and multi-scale rough structures are formed [31-33]. The presence of these micro- and nanostructures is responsible for lower surface energy (or higher CA), as they promote the formation of air pockets between the aqueous droplet and the sample surface [34]. However, when the multiscale structures agglomerate, the surface hydrophobicity may decrease [28]. An et al. reported that the CA of cerium/stearic acid composite coatings on aluminium alloy depends on the Ce/SA ratio in the formation solution [28]. Similar to the results shown in Fig. 2, they showed an increase and then a decrease in the CA value with the increase of Ce/SA relation. According to the authors, this behaviour is related to the morphology of the coatings. The formation of micro/nanoparticles leads to hydrophobic surfaces. However, as the

cerium/stearic acid ratio increases, the particles agglomerate leading to a decrease in the CA measurement. Therefore, it could be concluded that the 0.50 mmol/L SA treatment is not sufficient to cover the entire surface with multi-scale structures, while increasing the SA concentration to 1.00 mmol/L leads to a higher deposition of SA, which after evaporation of ethanol leads to an agglomerated structure that does not exhibit hydrophobic properties. Hence, the 0.75 mmol/L SA bath treatment is the optimal one to obtain hydrophobic coatings.

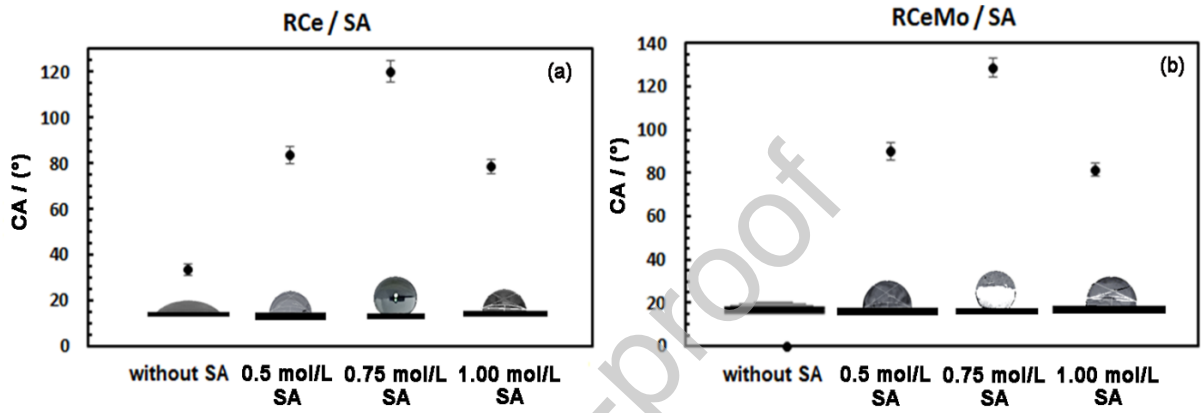

Fig. 1 Contact angles (CA) with Ringer solution for AZ91D Mg alloy coated with **(**a) RCe-HAsc untreated (without SA) and treated with different concentrations of SA, (b**)** RCeMo-H_3Cit untreated (without SA) and treated with different concentrations of SA.

In order to evaluate the anticorrosive properties of the SA-modified coatings, Tafel polarization curves for the uncoated and coated Mg alloy are presented (Fig. 2), and the parameters obtained from the extrapolation of the curves are listed in Table 1. In previous works, we presented the curve for the untreated AZ91D Mg alloy [29,30], and from its extrapolation, the obtained values for E_{corr} and i_{corr} were -1.501 ± 0.050 V vs $Ag/AgCl_{sat}$ and 0.1050 ± 0.0050 mA cm^{-2}, respectively. The results for the RCe-HAsc and the RCeMo-H_3Cit have been published previously and are shown here with comparative purposes [29,30]. Both cerium-based simple coatings reduce the corrosion rate of the substrate in Ringer solution. As it was reported, the coatings are composed of cerium oxides and hydroxides [29,30], and their anticorrosive properties are related to the barrier effect and to the self-healing effect of the cerium ions, which

combines with the OH^- produced during the corrosion process to form cerium compounds that precipitate onto the substrate surface. In Tafel polarization, the i_{corr} is a dynamic category parameter directly related to the corrosion rate [35]. After the post-treatment of the RCe-HAsc coated sample, it was found that immersion in the SA baths of different concentrations improved the corrosion resistance of the cerium-based simple coating (Fig. 2(A)). Treatment in 0.75 mmol/L SA diminishes the i_{corr} value by two orders of magnitude compared to the RCe-HAsc coating. A similar behaviour is noted for the post-treatments of the RCeMo-H_3Cit coating (Fig. 2(B)), where the treatment in 0.75 mmol/L SA gives the duplex coating with the best corrosion resistance. These results are in agreement with the measurement of CA, where treatment in 0.75 mmol/L SA gave higher values between the different SA baths, suggesting that, in addition to the barrier effect of the duplex coating, the hydrophobic nature of the surface prevents penetration of the solution [21,27]. On the other hand, E_{corr} is a thermodynamic parameter that represents the tendency of corrosion reactions to occur. It is defined as the potential at which the rates of cathodic and anodic electrochemical reactions are equal [36]. It can be seen from Table 2 that the values of E_{corr} increase after the SA treatment in all cases, but they remain nobler than that of the AZ91D alloy. The change in surface morphology after SA treatment could lead to a change in equilibrium and then a shift in corrosion potential [36].

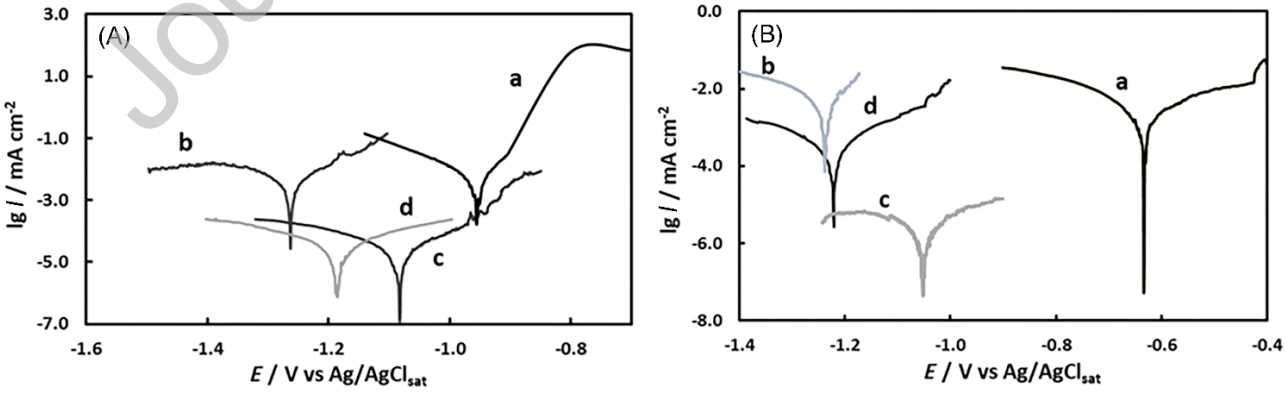

Fig. 2. Tafel polarization curves in Ringer solution for the bare AZ91D Mg alloy coated with (A): (a) RCe-HAsc untreated and treated in (b) 0.50 mmol/L SA, (c) 0.75 mmol/L SA and (d)

1.00 mmol/L SA, and (B): (a) RCeMo-H_3Cit untreated and treated in (b) 0.50 mmol/L SA, (c) 0.75 mmol/L SA and (d) 1.00 mmol/L SA.

Table 1 Tafel parameters for the cerium-based coatings untreated and treated in SA solutions.

Treatment	RCe-HAsc		RCeMo	
	E_{corr} / V	i_{corr} / mA cm^{-2}	E_{corr} / V	i_{corr} / mA cm^{-2}
Without SA	-0.952 ± 0.015	$5.400\times10^{-3} \pm 2.000\times10^{-4}$	-0.637 ± 0.020	$2.000\times10^{-3} \pm 1.000\times10^{-4}$
0.50 mol/L SA	-1,051 ± 0.075	$1.456\times10^{-3} \pm 1.804\times10^{-4}$	-1.237 ± 0.119	$1.560\times10^{-3} \pm 1.120\times10^{-4}$
0.75 mol/L SA	-1.081 ± 0.025	$2.119\times10^{-5} \pm 1.161\times10^{-6}$	-1.005 ± 0.019	$6.020\times10^{-6} \pm 1.650\times10^{-7}$
1.00 mol/L SA	-1.184 ± 0.119	$3.091\times10^{-5} \pm 3.824\times10^{-6}$	-1.220 ± 0.105	$3.100\times10^{-5} \pm 2.100\times10^{-6}$

Up to this point, it has been proved that it is possible to form an SA layer onto the samples coated with cerium-based simple coatings. However, direct coating of SA onto the uncovered AZ91D Mg alloy was not possible. The results reveal that increasing the SA concentration did not consistently enhance the CA and the corrosion resistance of the coatings. It could be suggested that the treatment in 0.50 mmol/L SA is not enough to attach the highest possible hydrophobicity. The treatment in 0.75 mmol/L SA produces a hydrophobic substrate surface. And in the presence of 1.00 mmol/L SA, the compound may exceed the necessary amount and does not adhere well to the cerium-based simple coating surface, resulting in a less protective duplex coating. Apparently, post-treatment of both cerium-based simple coatings in 0.75 mmol/L SA bath is the most effective for improving the CA and the anticorrosive properties. For practical purposes, the composite coatings will be called as RCe/SA and RCe-Mo/SA for the RCe-HAsc and RCeMoH_3Cit simple coatings treated in 0.75 mmol/L SA, respectively.

According to the reports of various authors, the cracked structure of the cerium-based simple coatings would allow the penetration of SA for the formation of hydrophobic coating [37,38]. Khalifeh et al. reported the formation of a hydrophobic stearic acid film onto an anodized high purified magnesium [37]. They demonstrated that immersion of the anodized substrate in an excess SA concentration bath was not effective in enhancing the anticorrosive properties of the coating. It was seen that a certain amount of SA is enough to create the hydrophobic surface.

Above this amount, the rest of the compound will precipitate onto the substrate surface during the treatment. However, the excess precipitate will be dissolved in the corrosive media without causing any protective effect.

3.2 Morphological and compositional characterization of the composite coatings

The superficial morphology and the elemental composition of the composite coatings were studied by SEM and EDX analysis (Figs. 3 and 4). After the formation onto AZ91D Mg alloy, both cerium-based simple coatings are yellow-coloured with a mud-cracked morphology which was already published (Figs. 3(a) and 4(a)) [29,30]. After the SA post-treatment, the colour of the surfaces is completely white, suggesting that the stearic acid modifies the surface. From the SEM images, it can be seen that the mud-cracked morphology of the cerium-based simple coatings [29,30,39] is covered by porous petal-like cluster structures corresponding to the SA deposit (Fig. 3(b)). EDX analysis of the RCe/SA shows the signals for Mg, Al and Ce (Fig. 3(d)) which could be associated with the cerium-based simple coating since it is composed of cerium oxides and Mg and Al corrosion products [29], and the C signal could be originated by the presence of SA. From Fig. 4(b) it is observed that the RCeMo/SA coating presents a more compact structure than the RCe/SA. The obtained EDX results (Fig. 4(d)) are similar to those of the RCe/SA coating with the addition of the Mo signal from the RCeMo simple coating. SEM micrographs of the cross-sectional view of the coatings were taken with the aim of evaluating the thickness of the coatings. However, as can be seen from Figs. 3(e) and 4(e), it is difficult to obtain a definite thickness value since the SA deposition is not uniform. For the RCe/SA coating, the thickness range is between 55 and 109 μm, whereas for the RCeMo/SA coating, thicknesses between approximately 46 and 85 μm were measured. This type of non-uniform thickness has been previously reported for other stearic acid-based coatings [32].

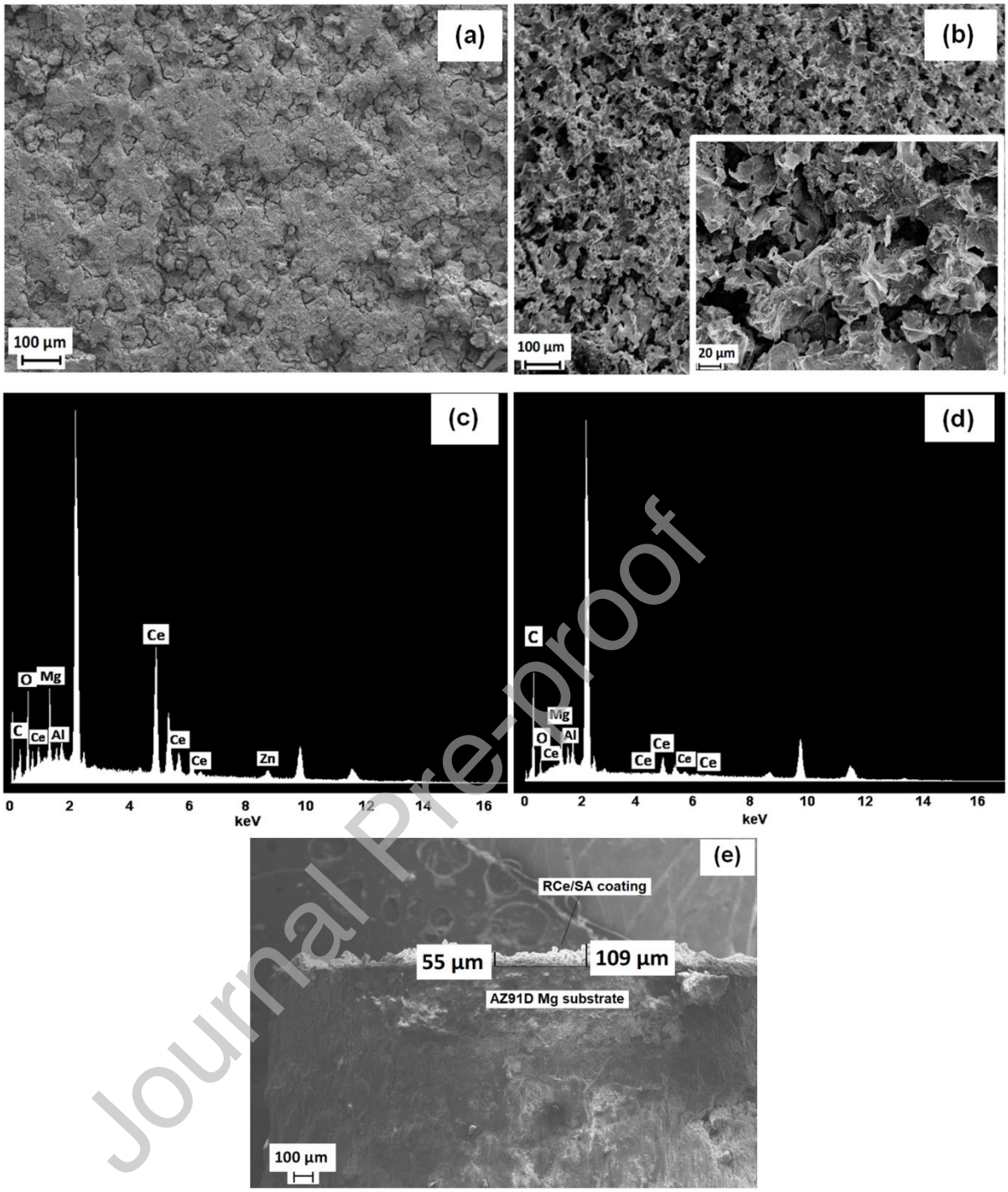

Fig. 3. SEM micrographs of the AZ91D Mg alloy covered with the (a) RCe and (b) RCe/SA coatings, EDX spectra of the AZ91D Mg alloy covered with the (c) RCe and (d) RCe/SA coatings, (e) cross-sectional view of the AZ91D Mg alloy covered with RCe/SA.

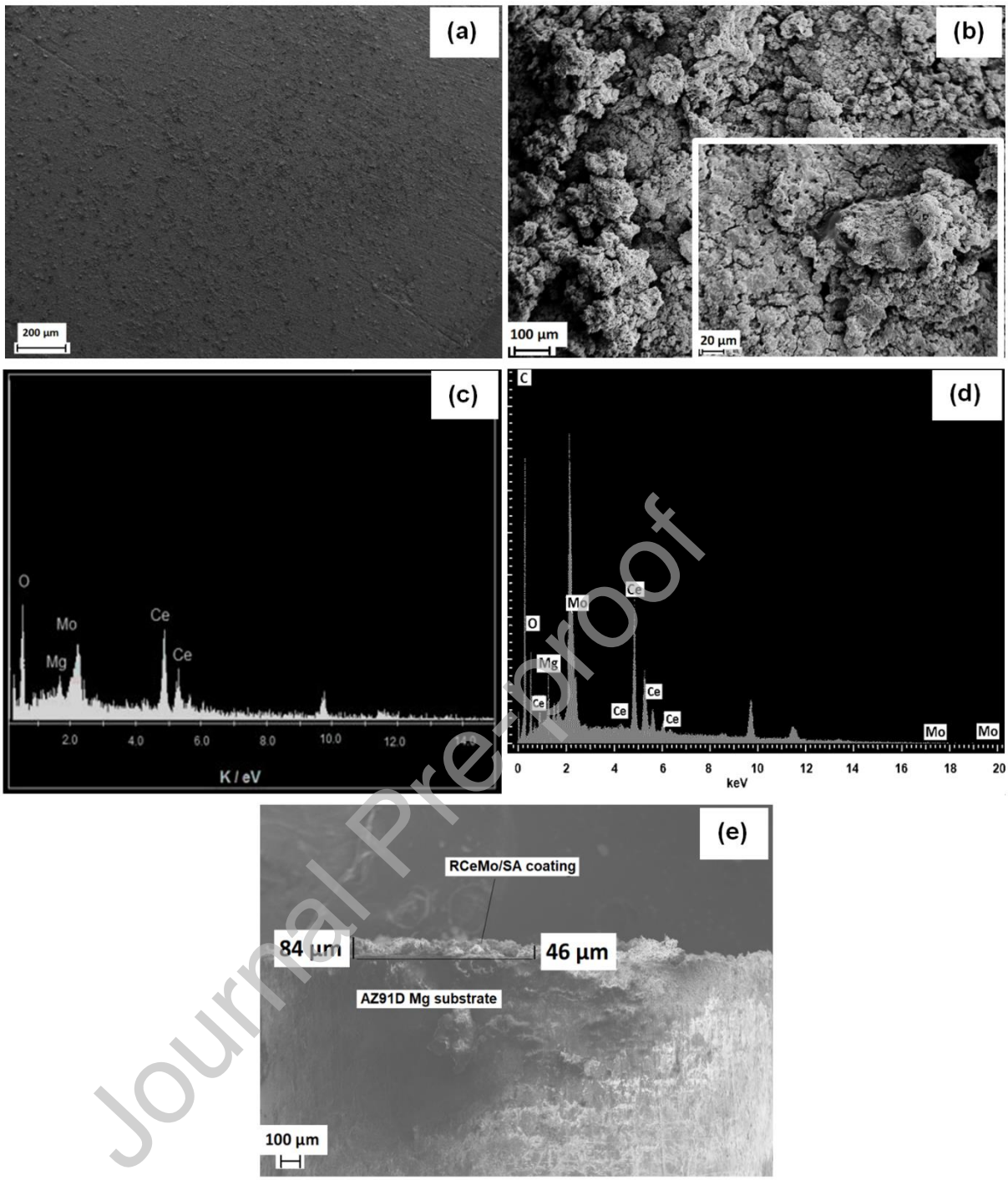

Fig. 4. SEM micrographs of the AZ91D Mg alloy covered with the (a) RCeMo and (b) RCeMo/SA coatings, EDX spectra of the AZ91D Mg alloy covered with the (a) RCeMo and (b) RCeMo/SA coatings, (e) cross-sectional view of the AZ91D Mg alloy covered with RCeMo/SA.

To further analyse the chemical composition of the hydrophobic coatings, XPS analysis was carried out. Fig. 5 presents the XPS spectra for the SA-modified samples. From the wide scans, it can be seen that both coatings contain C and O. The Ce signal corresponding to the cerium-based simple coatings could be blocked by the SA layer on top since, as seen from Figs. 3(e) and 4(e), the thickness of the coatings is several tens of microns. Deconvolution of the C 1s peak shows the presence of C-O and C-C bonds, related to the presence of SA [19].

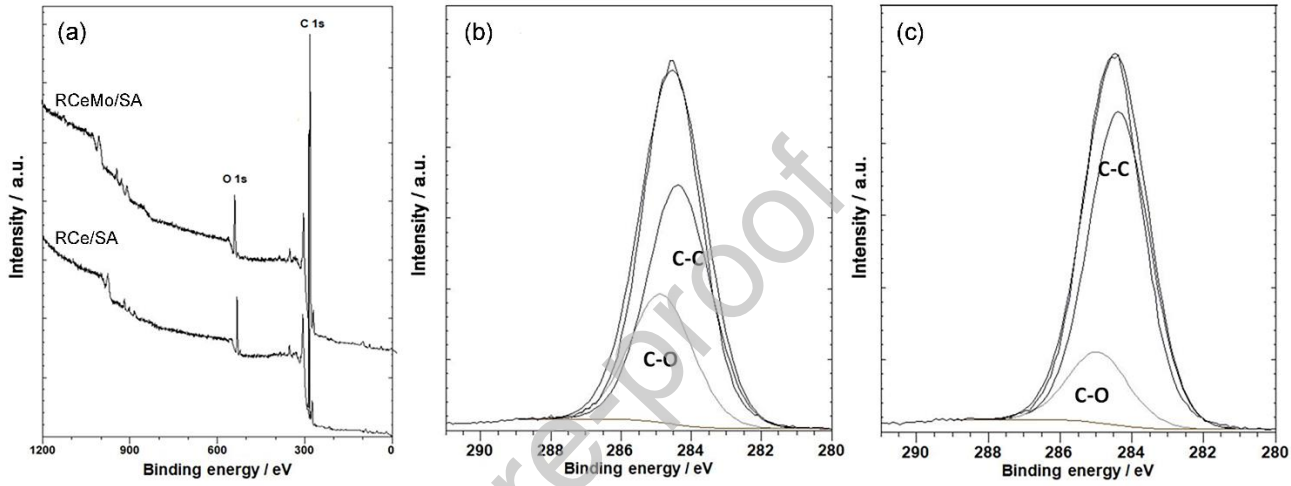

Fig. 5. (a) XPS survey spectra for the RCe/SA and RCeMo/SA samples, and higher resolution C 1s XPS spectra of **(**b**)** RCe/SA and **(**c**)** RCeMo/SA samples.

The ATR-FTIR analysis of the substrate uncovered and covered with the simple and duplex coatings was done in order to compare the chemical composition of the samples (Fig. 6). For both cerium-based simple coatings, the spectra obtained were very similar, hence one of them is showed as an example (Fig. 6(b)). As can be seen, there is no significant differences between the spectra of the cerium-based sample and the uncoated Mg alloy. After the post-treatment in SA bath (Fig. 6(c) and (d)), it is possible to identify different peaks, which are more intense in the case of the RCeMo/SA coating. Peaks at 2919 and 2850 cm^{-1} are attributed to the C-H stretching vibration of the SA [19,27,38]. Peaks at 1702 and 1470 cm^{-1} are related to carboxylic acid (C=O) vibration and symmetric carboxylate (COO^-) stretching vibration, respectively [27]. In addition, the broad band around 1315-1186 cm^{-1} in spectrum d could be associated with the presence of aliphatic long-chain carboxylic acids. On the other hand, the peak at 1573 cm^{-1}

could be attributed to asymmetric carboxylate (COO^-) stretching vibration, related to the presence of MgSt or CeSt [38]. These results confirm the modification of the cerium-based simple coatings after the post-treatment and suggest that the duplex coating could be composed of SA and MgSt [38]. According to the literature, when a cerium-based coated substrate is immersed in the SA bath, the compound diffuses into the cracks and pores of the simple coating [38]. As the cerium-based coatings are composed of Mg and Ce oxides and hydroxides, reactions with SA would take place to form magnesium and cerium stearates (MgSt and CeSt, respectively) [19,38]. MgSt and CeSt promote the bonding of SA with the surface, then, the outermost layer of the coating would be formed by a thin SA layer [38]. As a result, it could be assumed that the stearic acid would interact with the substrate surface in both ways, by chemical reactions and physical adsorption on the surface [19].

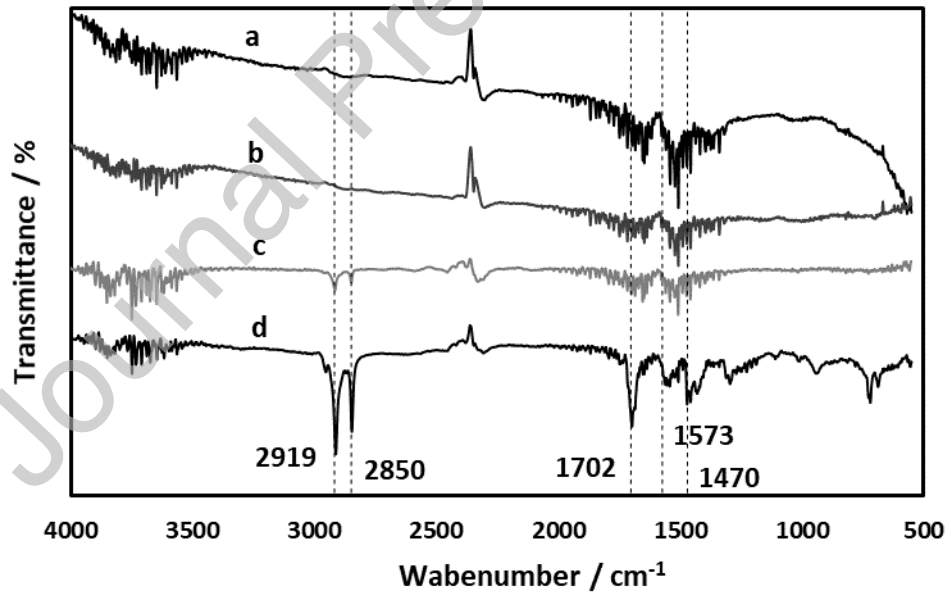

Fig. 6. ATR-FTIR spectra of the AZ91D Mg alloy: (a) uncovered, and covered with (b) cerium-based simple coating, (c) RCe/SA coating and (d) RCeMo/SA coating.

3.3 Anticorrosion performance of the composite coatings

Impedance measurements were recorded in order to evaluate the anticorrosive performance of the RCe/SA and RCe-Mo/SA duplex coatings. The curves for the untreated AZ91D Mg alloy

after 1 h of immersion are presented in Fig. 7. The Nyquist curve (Fig. 7(a)) is characterized by one capacitive semicircle and one inductive loop at low frequencies [11,12]. Fig. 9(a) depicts the equivalent circuit employed to simulate the impedance response. The R_S, R_{ct} and CPE represent the solution resistance, the charge transfer resistance and capacitive reactance, respectively [40,41]. Whereas R_L and L correspond to the inductive response. The obtained values from the simulation are presented in Table 2. On the other hand, Fig. 8 shows the Nyquist and Bode plots for the coatings at different immersion times. The curves for the RCe/SA samples (Fig. 8(a-c)) present two capacitive loops followed by an inductive loop. In general, the diameter of the capacitive arc is directly related to the corrosion resistance [42]. A larger diameter of the capacitive loop reflects better anticorrosive properties. On the other side, the inductive loop at low frequencies indicates the existence of an adsorption/desorption process on the surface, which is associated with the corrosion process [20]. From the Nyquist plots in Fig. 8, it could be seen that the diameter of the capacitive loop at the initial time is larger than that of the corresponding Mg alloy (Fig. 7(a)). Then, the diameter decreases with increasing exposure time. Up to 48 h of immersion, the RCe/SA coating still provides protection to the substrate in Ringer solution, but after 72 h, the protective properties deteriorate. The impedance Bode plots (Fig. 8(b)) show that, up to 48 h, the low-frequency impedance modulus $|Z|$ is larger than that obtained for the uncoated alloy (Fig. 7(b)), suggesting that the coating is protecting the alloy from corrosion [43]. As it was expected, the $|Z|$ decreases with increasing immersion time. From the phase angle plot (Fig. 8(c)) it can be noticed the existence of a small trough close to 1 Hz is related to the inductive loop of the impedance response [41]. In order to better understand the impedance results, the curves were simulated employing the equivalent circuit presented in Fig. 9(b). The circuit consists of two constant phase elements due to the intrinsic inhomogeneity of the coating [44] and an inductance. Usually, the behaviour at high-medium frequencies is associated with the outer layer, while the electrochemical behaviour at low frequencies is related to the interface between the substrate and the coating [19]. In this case,

the R_S represents the solution resistance; the CPE_c and R_c are associated with the capacitance and resistance of the duplex coating; the CPE_{dl} and R_{ct} fit the electronic double-layer capacitance and charge-transfer resistance; and L and R_L are attributed to the inductive behaviour and the resistance caused by the degradation [19,41,42]. The fitted parameters are listed in Table 2. Comparing the R_{ct} values obtained for the uncoated substrate and the RCe/SA coating, it is clear that the presence of the duplex coating enhances the corrosion resistance of the sample, as it exhibits higher values throughout the immersion time [40]. According to the proposed circuit, the diameter of the capacitive loop in Nyquist plot is equal to $R_c + R_{ct}$, whereas the sum of R_S, R_c and R_{ct} represents the $|Z|$ at low frequency [45]. Since the corrosion resistance is correlated to the diameter of capacitive loop and to the impedance modulus at low frequencies, the values of R_c and R_{ct} are expected to be high at initial immersion times and then decrease at longer immersion times [41,45].

In the case of the RCeMo/SA coating, the Nyquist curves show the same behaviour with two capacitive loops and one inductive loop at low frequencies (Fig. 8(d)). After 72 h of immersion in Ringer solution, the diameter of the capacitive loop remains larger than that of the corresponding uncoated AZ91D alloy (Fig. 7(a)), indicating better corrosion resistance. The $|Z|$ value at low frequencies and the maximum value of the phase angle decrease with the increasing immersion time (Fig. 8(e) and (f)), denoting a slow deterioration of the protective properties of the RCeMo/SA coating. The equivalent circuit used for the simulation is the same as for the RCe/SA coating (Fig. 9(b)) and the fitted parameters are presented in Table 2. When the CPE has a value of $n = 1$, it represents an ideal capacitor. Again, the comparison of the R_{ct} values of the uncoated sample and the RCeMo/SA coated sample shows that the values for the coated sample are higher than that for the uncoated sample during the 72 h of immersion time. This indicates that the composite coating enhances the corrosion resistance of the alloy. Furthermore, from the comparison of the R_{ct} values for both duplex coatings, it is noticed that the RCeMo/SA coating presents higher values than the RCe/SA coating for all the immersion times, indicating

that the RCeMo/SA duplex coating protects the substrate to a greater extent. Table 2 also shows that the fitting parameters first decrease and then increase with the immersion time. It has been reported that the increase in CPE_c value along the exposure time is related to solution penetration in the coating [46]. In this case, the results are in agreement with those presented by other authors [28,47], where there are two different stages in the impedance measurement. According to the literature, this behaviour could be related to the self-healing properties of the cerium-based coating [13]. When the aggressive medium penetrates the coating, cerium ions are released. These ions combine with the OH^- present in the environment to form oxides and hydroxides, which are deposited on the substrate surface and provide corrosion protection. Therefore, after a certain immersion time, an improvement in the corrosion resistance of the sample was observed.

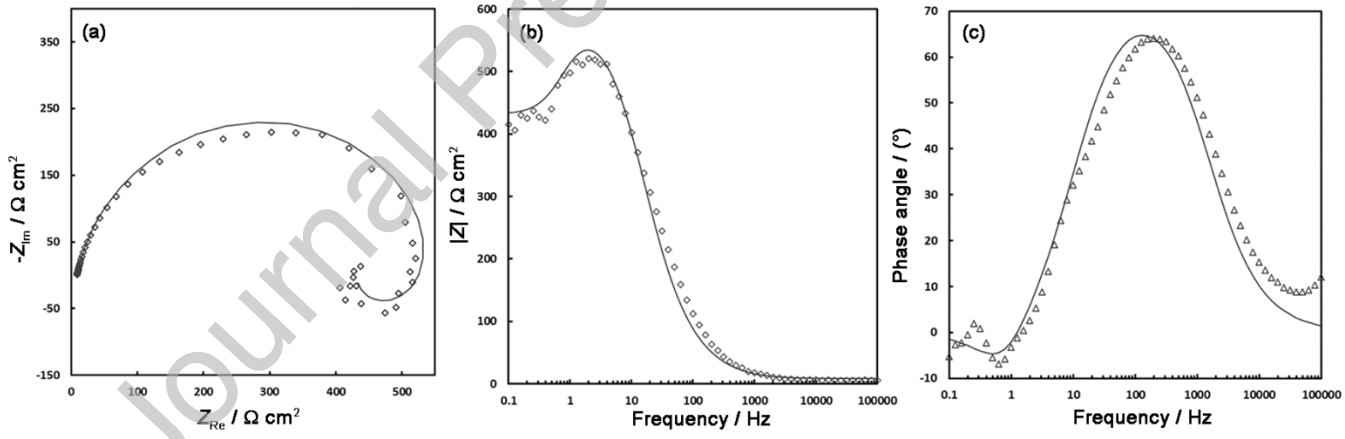

Fig. 7. Impedance responses obtained in Ringer solution for the bare AZ91D Mg alloy after 1 h of immersion: (a) Nyquist plot, (b, c) Bode plots.

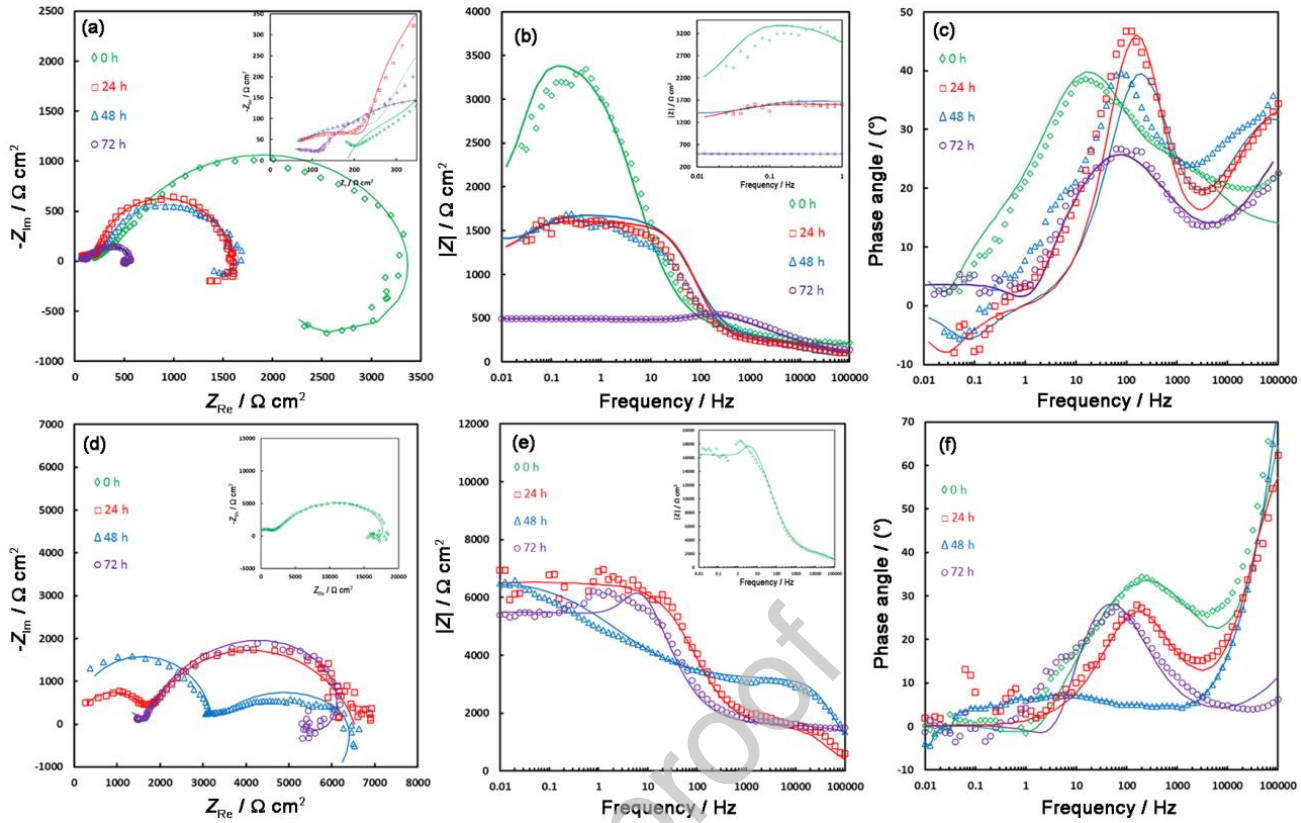

Fig. 8. (a, d**)** Nyquist, (b, e) impedance Bode and **(**c, f**)** phase Bode plots for the AZ91D Mg alloy covered with the (a-c) RCe/SA and (d-f) RCeMo/SA coatings.

Table 2 Fitted parameters of impedance results of the uncoated and coated alloy in Ringer solution for different immersion time.

Sample	R_S / Ω cm^2	CPE$_c$/ F cm^{-2}	n_c	R_c / Ω cm^2	CPE$_{dl}$ / F cm^{-2}	n_{dl}	R_{ct} / Ω cm^2	R_L / Ω cm^2
Mg AZ91D	8.5	3.17×10^{-5}	0.87	414.4	-	-	-	150
RCe/SA								
0 h	182.6	8.07×10^{-6}	0.75	300.0	2.68×10^{-5}	0.75	3072.0	3063.3
24 h	28.6	6.90×10^{-6}	0.62	290.5	2.81×10^{-6}	0.91	1350.8	5090.0
48 h	22.6	2.81×10^{-6}	0.63	245.5	2.11×10^{-6}	0.99	1350.8	3990.7
72 h	15.1	1.52×10^{-6}	0.66	91.5	1.04×10^{-4}	0.60	573.4	1282.9
RCeMo/SA								
0 h	10.0	1.67×10^{-9}	1.0	1850.0	1.77×10^{-6}	0.63	19013.0	65315

24 h	81.7	6.61×10^{-9}	0.93	1643.5	1.74×10^{-6}	0.78	6673.8	17065
48 h	0.05	1.18×10^{-9}	1.0	3148.5	7.76×10^{-5}	0.51	3507.1	74.0
72 h	6.6	5.38×10^{-7}	0.60	1628.5	4.60×10^{-6}	0.77	5940.0	11036

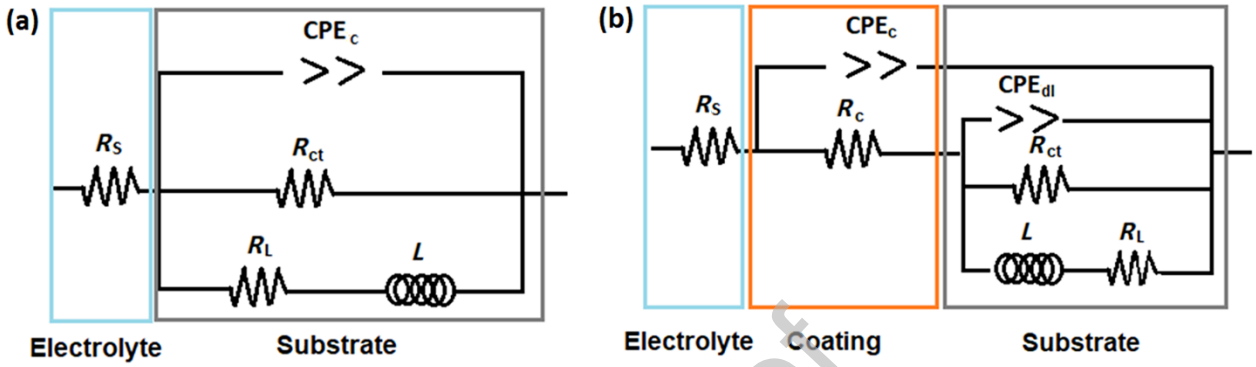

Fig. 9. Fitted equivalent circuits employed to analyse EIS data of (a) uncoated AZ91D Mg alloy after 1 h of immersion and (b) RCe/SA and RCeMo/SA coated Mg alloy after different immersion times in Ringer solution.

From the simulation parameters, the polarization resistance (R_P) for the coatings can be calculated based on the employed circuit model [42]. The values obtained for the coated samples at the initial immersion time were 250.1 and 1850.0 Ω cm^2 for RCe/SA and RCeMo/SA, respectively. These results are in agreement with the impedance curves, where it is noticeable that the RCeMo/SA coating provides a higher protection degree to the Mg substrate.

$$\frac{1}{R_p} = \frac{1}{R_c + (R_{ct}^{-1} + R_L^{-1})} \quad (1)$$

It is known that Mg corrosion in aqueous solution produces H_2 gas, as can be seen from the global corrosion reaction (Eq. (2)). Usually, the corrosion products do not affect the gas evolution, so measuring the hydrogen released volume is a reliable method to evaluate substrate

degradation [48]. Fig. 10 presents the evolution of H_2 gas in Ringer solution over time. It is clear that both composite coatings reduce the hydrogen evolution rate on the substrate compared to the uncoated sample. At the initial immersion times, the H_2 evolution for the uncoated sample seems to be low. This is related to the $Mg(OH)_2$ protective layer that forms on the Mg substrate surface [49]. However, this film is weak and dissolves rapidly in Ringer solution. When the hydroxide film breaks down, the substrate comes into direct contact with the corrosive medium and begins to corrode. For the coated specimens, the corrosion process must go through the degradation of the coating. It is expected that the coating blocks the contact between the substrate and the corrosive solution. First, the corrosive ions would penetrate through the SA layer and get in contact with the cerium-based coating, which would avoid direct contact with the substrate. However, the presence of some defects such as pores or cracks would lead to the creation of paths for the solution to get in contact with the substrate surface. Then, the corrosion process starts at the interface between the Mg alloy surface and the coating, where the $Mg(OH)_2$ layer is formed [49]. The accumulation of corrosion products may lead to cracking and peeling off of the coating. In addition, the released hydrogen promotes the degradation of the coating. Therefore, the corrosion rate of the coated substrates would increase with immersion time. Nevertheless, it is clear that the hydrogen evolution of the RCe/SA and RCeMo/SA samples is significantly lower than that of the uncoated Mg.

$$Mg + 2H_2O \longrightarrow Mg(OH)_2 + H_2 \qquad (2)$$

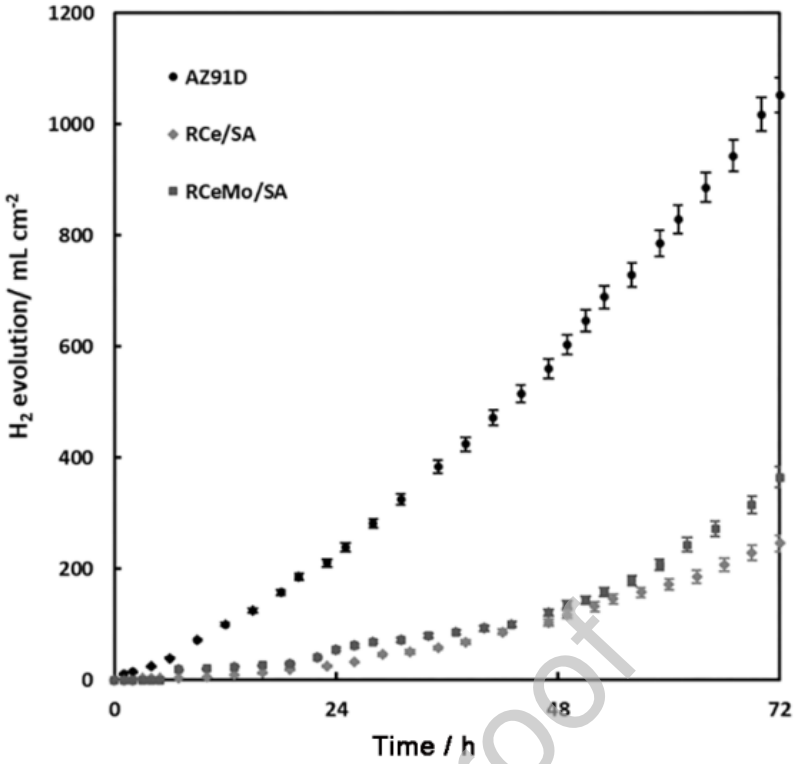

Fig. 10. Hydrogen evolution volume of the uncoated and coated samples in Ringer solution.

In an effort to corroborate the electrochemical results, the release of Mg in Ringer solution was measured after different exposure times of the samples. The obtained values are presented in Table 3. As can be seen, both SA-modified samples significantly retard the dissolution of the substrate in the corrosive media, verifying the protective properties of the cerium-based/SA duplex coatings. The released Mg concentration for RCe/SA is slightly lower than that for RCeMo/SA, which is in agreement with the H_2 evolution measurements at the initial immersion times. With increasing immersion time, the RCeMo/SA sample shows slightly better protective behaviour with lower Mg release, which is consistent with the impedance results.

Table 3 Mg released in Ringer solution after different immersion time of the samples.

Immersion time / h	Mg released / mg · L^{-1}		
	Mg AZ91D	RCe/SA	RCeMo/SA
5	3.90	0.24	0.40
24	4.60	0.77	0.43
48	-	0.91	0.59
72	-	1.05	0.76

The evaluation of the hydrophobicity of the surface along the exposure time is of interest to clarify what happens as the coatings are being corroded in Ringer solution. Fig. 11 depicts the evolution of CA during the immersion time in Ringer solution. Clearly, for both duplex coatings, the CA decreases with the immersion time, and no CA was measured after 48 h of exposure. The decrement of the CA may be related to the desorption of the SA layer in the corrosive media [19]. It is worth mentioning that the decrement in the CA is faster for the RCeMo/SA coating than for the RCe/SA. On the other hand, from the impedance results, it was noticed that the corrosion resistance decreased earlier in the case of the RCe/SA coating. This suggests that even though the hydrophobicity of the surface contributes to enhancing the anticorrosive properties, it is not the only contributing factor to the corrosion protection. The properties of the inner cerium-based simple coating also influence the behaviour of the composite coating. An et al., who reported the formation of a cerium-based superhydrophobic coating, proposed the existence of a synergistic effect of the anti-wetting properties of the hydrophobic coating and the corrosion inhibition effect of the cerium ions [28]. Between the simple cerium-based coatings, the RCeMo-H_3Cit has better anticorrosive properties than the RCe-HAsc (Table 1) [29,30], resulting in better protective conditions for the sample before SA post-treatment.

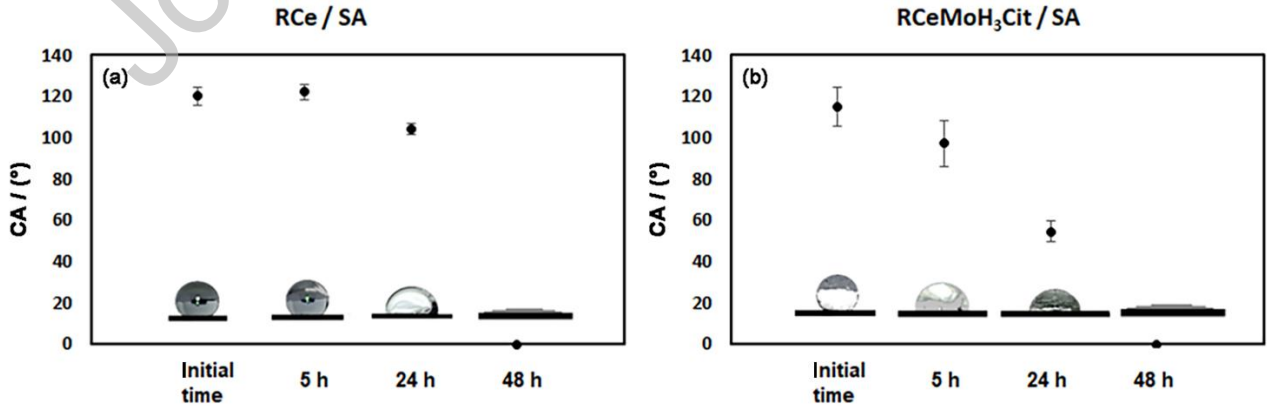

Fig. 11. Contact angles (CA) for AZ91D Mg alloy coated with (a) RCe/SA and (b) RCeMo/SA after different immersion time in Ringer solution.

To better understand the effects of the aggressive media on the morphology of the coatings, SEM micrographs of RCe/SA and RCeMo/SA were taken after different immersion times in Ringer solution (Fig. 12). When the specimens were removed from the corrosive medium, the surfaces showed a white color to the naked eye. By comparison with Fig. 3 (sample before immersion), it can be seen that the surface of the RCe/SA duplex coating (Fig. 12(a)) shows no significant change after 24 h of immersion. It still exhibits a petal-like sheet structure already shown for other SA coatings [18]. In the case of the RCeMo/SA composite coating after 24 h of immersion (Fig. 12(b)), by comparison with Fig. 4 (before immersion) the change in the morphology is noticeable. The stearic acid layer exhibits a smooth globular morphology. The absence of nano or microstructures leads to hydrophilicity [28,34]. It can be inferred that the significant change in CA value for the RCeMo/SA sample after 24 h of immersion in Ringer solution is related to the change in surface morphology, while the laminar structure of the RCe/SA coating contributes to hydrophobicity and maintains a CA > 90° even after 24 h of immersion. Fig. 12(c) and (d) exhibits the surfaces of the duplex coatings after 72 h of immersion in Ringer solution. Some micro-holes were observed on the surface of the sample coated with RCe/SA. EDX analysis of the zone (Fig. 12(e)) presents a strong signal for Mg, indicating that the coating was severely damaged. On the other hand, from SEM images, the RCeMo/SA coated sample shows no signs of extreme damage. The EDX spectrum (Fig. 12(f)) exhibits the presence of Ce from the coating and a weaker Mg signal. In both cases, signals of Cl, Ca, K and Na are related to Ringer solution, suggesting the existence of corrosion products on the surfaces.

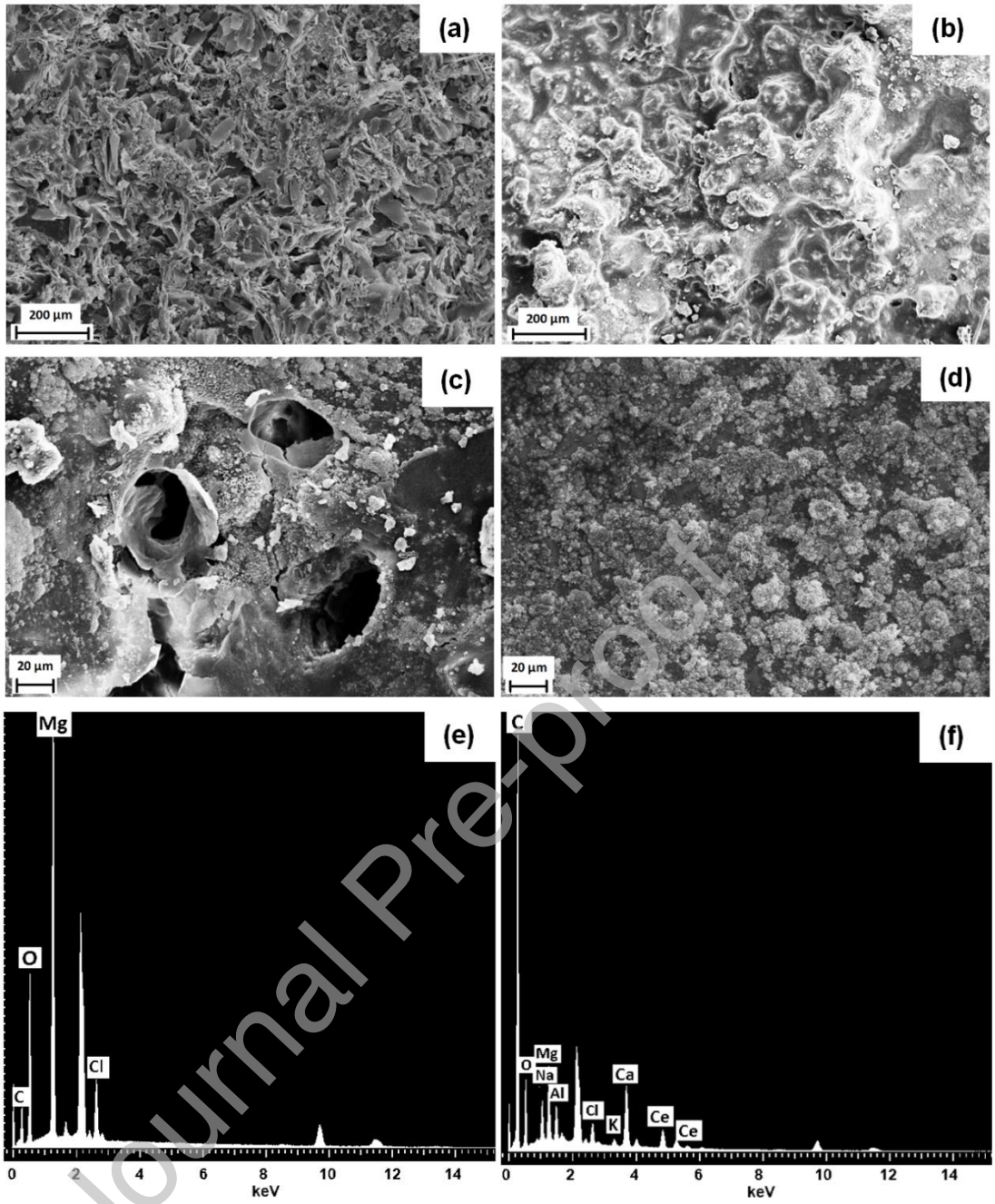

Fig. 12. SEM micrographs of the surface of (a, c) RCe/SA, and (b, d) RCeMo/SA duplex coatings after immersion for (a, b) 24 h and (c, d) 72 h in Ringer solution, and EDX spectra of (e) RCe/SA and (f) RCeMo/SA samples after 72 h of immersion.

The adhesion of coatings to the substrate surface is an important factor in corrosion protection. To evaluate the effect of corrosive media on duplex coating adhesion, a peel-off test was performed after immersing the specimens in Ringer solution for 24 h. Fig. 13 depicts the SEM

micrographs of the samples after the test. Both the RCe/SA and RCeMo/SA composite coatings show some delaminated areas and other intact areas. There is no evidence of uncovered areas, indicating that there is good adhesion between the substrate and the coating even after exposure to the corrosive media. In addition, some structures of the outer SA layer can be seen in the higher magnification images in both cases, indicating good adhesion between the cerium-based coatings and the SA coating [32].

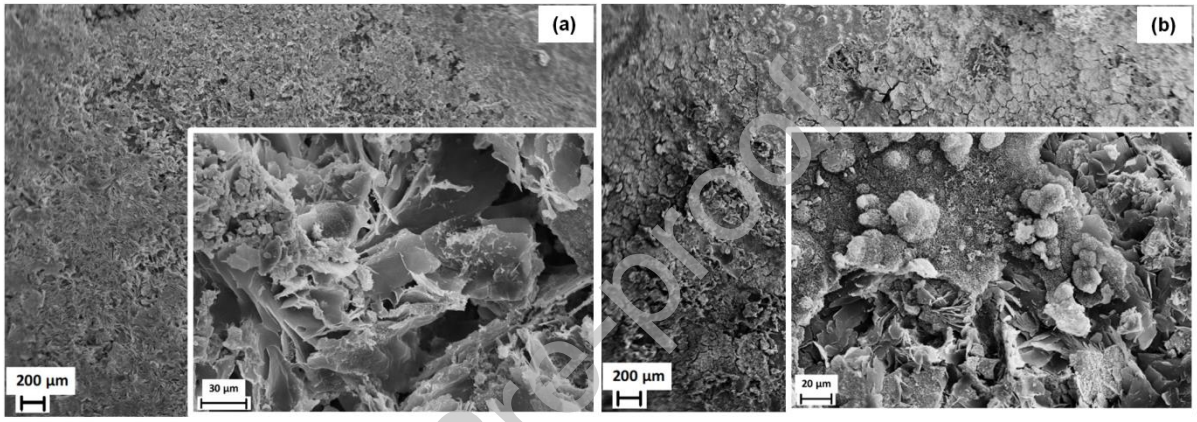

Fig. 13. SEM micrographs of (a) RCe/SA and (b) RCeMo/SA surface samples after 24 h of immersion in Ringer solution and posterior peel-off test.

By evaluating the duplex coatings after immersion in Ringer solution, the impedance and CA results can be explained. From the SEM micrographs, it was seen that the RCe/SA coating maintains its morphology after 24 h of immersion, resulting in the hydrophobic property being maintained. However, after 72 h it is corroded and damaged by the aggressive media, leading to a loss of its anticorrosive properties. This reinforces the idea that the hydrophobic properties of a coating contribute to the anticorrosive properties but are not the only factor that affects them. In addition, there was no significant delamination of the duplex coating after Ringer exposure, suggesting that coating failure is caused by damage to the coating structure rather than loosening of adhesion. On the other hand, the RCeMo/SA coating changes its morphology after 24 h of immersion, resulting in the loosening of hydrophobic properties. However, the

good adhesion and more compact structure of the RCeMo/SA composite coating may contribute to better anticorrosive properties than the RCe/SA duplex coating. Furthermore, the RCeMo simple coating seems to exhibit self-healing properties, which contributes to good corrosion resistance during the immersion period.

4. Conclusions

The combination of cerium-based simple coating anticorrosive properties with hydrophobic properties of SA was achieved. The formation of hydrophobic composite coatings onto AZ91D Mg alloy was done by the generation of the cerium-based simple coatings onto the substrate surface and their posterior immersion in SA bath. The concentration of the SA bath was found to affect the degree of hydrophobicity of the surfaces. For both cerium-based simple coatings studied, the optimum concentration to obtain a CA > 90° was 0.75 mmol/L SA. Moreover, the same concentration of SA bath for the post-treatment was most effective in enhancing the corrosion resistance of the substrate. In this way, two hydrophobic protective duplex coatings were effectively generated onto the substrate. The anticorrosive properties were attributed to the barrier effect of the composite coatings, the protective properties of the cerium compounds in the cerium-based simple coating, and the anti-wetting properties of the hydrophobic surface during the initial immersion stage.

In the following work, the coated samples will be investigated in *in vivo* tests.

Acknowledgments

This work was financially supported by CONICET (No. PIP11220200102064CO), ANPCYT (No. PICT 2019-02758) and Universidad Nacional del Sur (No. PGI 24/M159), Bahía Blanca, Argentina.

Declaration of competing interests:

The authors declare that they have no known competing financial interests or personal relationships that could have appeared to influence the work reported in this paper.

References

[1] M. Ali, M.A. Hussein, N. Al-Aqeeli, Magnesium-based composites and alloys for medical applications: A review of mechanical and corrosion properties, J. Alloy. Compd. 792 (2019) 1162-1190.

[2] J. Dong, T. Lin, H. Shao, H. Wang, X. Wang, K. Song, Q. Li, Advances in degradation behavior of biomedical magnesium alloys: A review, J. Alloy. Compd. 908 (2022) 164600.

[3] V. Kaushik, B. Nithish Kumar, S. Sakthi Kumar, M. Vignesh, Magnesium role in additive manufacturing of biomedical implants – Challenges and opportunities, Addit. Manuf. 55 (2022) 102802.

[4] J.L. Zhao, H.R. Cui, Z.Y. Gao, Y.Z. Bi, Z.Z. Dong, Y. Li, C.Q. Wang, Anticorrosive and antibacterial smart integrated strategy for biomedical magnesium, J. Magnes. Alloy. 11 (2023) 2789-2800.

[5] P. Tong, Y. Sheng, R. Hou, M. Iqbal, L. Chen, J. Li, Recent progress on coatings of biomedical magnesium alloy, Smart Mater. Med. 3 (2022) 104-116.

[6] Z.-Q. Zhang, Y.-X. Yang, J.-A. Li, R.-C. Zeng, S.-K. Guan, Advances in coatings on magnesium alloys for cardiovascular stents – A review, Bioact. Mater. 6 (2021) 4729-4757.

[7] L. Zhang, E.A.A. Mohammed, A. Adriaens, Synthesis and electrochemical behavior of a magnesium fluoride-polydopamine-stearic acid composite coating on AZ31 magnesium alloy, Surf. Coat. Technol. 307 (2016) 56-64.

[8] M. Razavi, M. Fathi, O. Savabi, D. Vashaee, L. Tayebi, In vivo assessments of bioabsorbable AZ91 magnesium implants coated with nanostructured fluoridated hydroxyapatite by MAO/EPD technique for biomedical applications, Mater. Sci. Eng. C 48 (2015) 21-27.

[9] S. Singh, G. Singh, N. Bala, Electrophoretic deposition of Fe_3O_4 nanoparticles incorporated hydroxyapatite-bioglass-chitosan nanocomposite coating on AZ91 Mg alloy, Mater. Today Commun. 26 (2021) 101870.

[10] W.F. Ng, M.H. Wong, F.T. Cheng, Cerium-based coating for enhancing the corrosion resistance of bio-degradable Mg implants, Mater. Chem. Phys. 119 (2010) 384-388.

[11] X. Cui, Y. Yang, E. Liu, G. Jin, J. Zhong, Q. Li, Corrosion behaviors in physiological solution of cerium conversion coatings on AZ31 magnesium alloy, Appl. Surf. Sci. 257 (2011) 9703-9709.

[12] S. Arthanari, K.S. Shin, A simple one step cerium conversion coating formation on to magnesium alloy and electrochemical corrosion performance, Surf. Coat. Technol. 349 (2018) 757-772.

[13] L.M. Calado, M.G. Taryba, Y. Morozov, M.J. Carmezim, M.F. Montemor, Novel smart and self-healing cerium phosphate-based corrosion inhibitor for AZ31 magnesium alloy, Corros. Sci. 170 (2020) 108648.

[14] B. Ramezanzadeh, M. Rostami, The effect of cerium-based conversion treatment on the cathodic delamination and corrosion protection performance of carbon steel-fusion-bonded epoxy coating systems, Appl. Surf. Sci. 392 (2017) 1004-1016.

[15] S. Hariprasad, S. Gowtham, S. Arun, M. Ashok, N. Rameshbabu, Fabrication of duplex coatings on biodegradable AZ31 magnesium alloy by integrating cerium conversion (CC) and plasma electrolytic oxidation (PEO) processes, J. Alloy. Compd. 722 (2017) 698-715.

[16] E.J. Falde, S.T. Yohe, Y.L. Colson, M.W. Grinstaff, Superhydrophobic materials for biomedical applications, Biomaterials 104 (2016) 87-103.
[17] R. Kumar, A.K. Sahani, Role of superhydrophobic coatings in biomedical applications, Mater. Today Proc. 45 (2021) 5655-5659.
[18] X. Liu, T.C. Zhang, H. He, L. Ouyang, S. Yuan, A stearic Acid/CeO2 bilayer coating on AZ31B magnesium alloy with superhydrophobic and self-cleaning properties for corrosion inhibition, J. Alloy. Compd. 834 (2020) 155210.
[19] G. Wang, D. Song, Y. Qiao, J. Cheng, H. Liu, J. Jiang, A. Ma, X. Ma, Developing super-hydrophobic and corrosion-resistant coating on magnesium-lithium alloy via one-step hydrothermal processing, J. Magnes. Alloy. 11 (2021) 1422-1439.
[20] M.A. Kamde, Y. Mahton, P. Saha, A stearic acid/polypyrrole-based superhydrophobic coating on squeeze-cast Mg-Sr-Y-Ca-Zn alloys for improved salt-water corrosion, Surf. Coat. Technol. 448 (2022) 128890.
[21] Y. Xu, D. Gao, Q. Dong, M. Li, A. Liu, X. Wang, S. Wang, Q. Liu, Anticorrosive behavior of epoxy coating modified with hydrophobic nano-silica on phosphatized carbon steel, Prog. Org. Coat. 151 (2021) 106051.
[22] P. Wan, J. Wu, L. Tan, B. Zhang, K. Yang, Research on super-hydrophobic surface of biodegradable magnesium alloys used for vascular stents, Mater. Sci. Eng. C 33 (2013) 2885-2890.
[23] J. Xie, J. Hu, L. Fang, X. Liao, R. Du, F. Wu, L. Wu, Facile fabrication and biological properties of super-hydrophobic coating on magnesium alloy used as potential implant materials, Surf. Coat. Technol. 384 (2020) 125223.
[24] A. Katdare, S. Thakkar, S. Dhepale, D. Khunt, M. Misra, Fatty acids as essential adjuvants to treat various ailments and their role in drug delivery: A review, Nutrition 65 (2019) 138-157.
[25] S. Mukherjee, M. Edmunds, X. Lei, M.F. Ottaviani, K.P. Ananthapadmanabhan, N.J. Turro, Stearic acid delivery to corneum from a mild and moisturizing cleanser, J. Cosmet. Dermatol. 9 (2010) 202-210.
[26] A. Patti, H. Lecocq, A. Serghei, D. Acierno, P. Cassagnau, The universal usefulness of stearic acid as surface modifier: applications to the polymer formulations and composite processing, J. Ind. Eng. Chem. 96 (2021) 1-33.
[27] M. Zhang, M. Zhao, R. Chen, J. Liu, Q. Liu, J. Yu, R. Li, P. Liu, J. Wang, Fabrication of the pod-like KCC-1/TiO_2 superhydrophobic surface on AZ31 Mg alloy with stability and photocatalytic property, Appl. Surf. Sci. 499 (2020) 143933.
[28] K. An, Y. Sui, Y. Wang, Y. Qing, C. Long, X. Liu, Y. Shang, C. Liu, Synergistic control of wetting resistance and corrosion inhibition by cerium to enhance corrosion resistance of superhydrophobic coating, Colloids Surf. A 653 (2022) 129874.
[29] A.P. Loperena, I.L. Lehr, S.B. Saidman, Formation of a cerium conversion coating on magnesium alloy using ascorbic acid as additive. Characterisation and anticorrosive properties of the formed films, J. Magnes. Alloy. 4 (2016) 278-285.
[30] I.L. Lehr, S.B. Saidman, Corrosion protection of AZ91D magnesium alloy by a cerium-molybdenum coating. The effect of citric acid as an additive, J. Magnes. Alloy. 6 (2018) 356-365.
[31] S. Masih, Z. He, X. Wang, P. Shen, W. Wang, M.D. Gilchrist, N. Zhang, Surface modification of WE43 magnesium alloy via alkali/stearic acid treatment for biodegradable drug-eluting stent applications, Mater. Chem. Phys. 308 (2023) 128249.
[32] F. Li, R. Sun, K. Chen, Construction and properties of a multifunctional stearic acid modified CeO2 coating on anodized AZ31B Mg alloy, J. Alloy. Compd. 945 (2023) 169316.
[33] L. Zhang, M. Zhang, J. Gao, M. Gao, X. Wang, B. Li, J. Liu, Study on the preparation and stearic acid modification of hydrophobic Ni625 laser cladding coating, Mater. Lett. 346 (2023) 134526.

[34] L. Zheng, S. Luo, S. Yang, Preparation of Cu/CuO@Stearic acid layer with superhydrophobicity to provide multiple barriers for corrosion protection of carbon steel, Mater. Chem. Phys. 306 (2023) 128048.
[35] H.R. Dong, Q. Li, D.B. Xie, W.G. Jiang, H.J. Ding, S. Wang, L.Y. An, Forming characteristics and mechanisms of micro-arc oxidation coatings on magnesium alloys based on different types of single electrolyte solutions, Ceram. Int. 49 (2023) 32271-32281.
[36] O.L. Li, M. Tsunakawa, Y. Shimada, K. Nakamura, K. Nishinaka, T. Ishizaki, Corrosion resistance of composite oxide film prepared on Ca-added flame-resistant magnesium alloy AZCa612 by micro-arc oxidation, Corros. Sci. 125 (2017) 99-105.
[37] S. Khalifeh, T.D. Burleigh, Super-hydrophobic stearic acid layer formed on anodized high purified magnesium for improving corrosion resistance of bioabsorbable implants, J. Magnes. Alloy. 6 (2018) 327-336.
[38] W.F. Ng, M.H. Wong, F.T. Cheng, Stearic acid coating on magnesium for enhancing corrosion resistance in Hanks' solution, Surf. Coat. Technol. 204 (2010) 1823-1830.
[39] A.P. Loperena, I.L.Lher, S.B. Saidman, Cerium coatings as an alternative for corrosion protection of AZ91D Mg alloy for biomedical applications, Adv. Mater. Sci. Res. 44 (2021) 1-24.
[40] G. Shen, L. Zhang, W. Wu, H. Wu, Z. Gu, S. Liu, G. Tan, X. Jie, Design and fabrication of enhanced corrosion-resistant LDH-Zn-G/Ni dual-layer structural coatings on magnesium alloys, J. Alloy. Compd. 917 (2022) 165475.
[41] M. Zhao, S. Wu, P. An, J. Luo, Study on the deterioration process of a chromium-free conversion coating on AZ91D magnesium alloy in NaCl solution, Appl. Surf. Sci. 253 (2006) 468-475.
[42] H. Fang, S. Zhou, X. Qi, C. Wang, Y. Tian, A multifunctional osteogenic system of ultrasonically spray deposited bone-active coatings on plasma-activated magnesium, J. Magnes. Alloy. 11 (2021) 2719-2739.
[43] Y. Dong, T. Wang, Y. Xu, Y. Guo, G. Li, J. Lian, A polydopamine-based calcium phosphate/graphene oxide composite coating on magnesium alloy to improve corrosion resistance and biocompatibility for biomedical applications, Materialia 21 (2022) 101315.
[44] M.U. Malik, M. Tabish, G. Yasin, M.J. Anjum, S. Jameel, Y. Tang, X. Zhang, S. Manzoor, S. Ibraheem, W.Q. Khan, Electroless codeposition of GO incorporated silane nanocomposite coating onto AZ91 Mg alloy: Effect of GO content on its morphology, mechanical and corrosion protection properties, J. Alloy. Compd. 883 (2021) 160790.
[45] Z. Fu, X. Chen, B. Liu, J. Liu, X. Han, Y. Deng, W. Hu, C. Zhong, One-step fabrication and localized electrochemical characterization of continuous Al-alloyed intermetallic surface layer on magnesium alloy, Coatings 8 (2018) 148.
[46] R. Parichehr, C. Dehghanian, A. Nikbakht, Preparation of PEO/silane composite coating on AZ31 magnesium alloy and investigation of its properties, J. Alloy. Compd. 876 (2021) 159995.
[47] S. Yang, R. Sun, K. Chen, Self-healing performance and corrosion resistance of phytic acid/cerium composite coating on microarc-oxidized magnesium alloy, Chem. Eng. J. 428 (2022) 131198.
[48] C.Y. Zhang, R.C. Zeng, C.L. Liu, J.C. Gao, Comparison of calcium phosphate coatings on Mg-Al and Mg-Ca alloys and their corrosion behavior in Hank's solution, Surf. Coat. Technol. 204 (2010) 3636-3640.
[49] Z. Ding, Q. Yuan, H. Wang, Y. Tang, Y. Tan, Q. He, Microstructure and properties of Nb2O5/Mg gradient coating on AZ31 magnesium alloy by magnetron sputtering, Ceram. Int. 49 (2023) 154-167.

Declaration of interests

☒ The authors declare that they have no known competing financial interests or personal relationships that could have appeared to influence the work reported in this paper.

☐The authors declare the following financial interests/personal relationships which may be considered as potential competing interests: